IEEE Access
Multidisciplinary | Rapid Review | Open Access Journal

Received 7 August 2023, accepted 31 August 2023, date of publication 8 September 2023, date of current version 22 September 2023.

Digital Object Identifier 10.1109/ACCESS.2023.3313561

RESEARCH ARTICLE

Practical Evaluation Method of Large Size IRS: Synthesis of Reflection Pattern of Sub-IRS

HIROMI MATSUNO, TAKUYA OHTO, (Member, IEEE), TOMOFUMI KANNO, AND TAKAHIRO HAYASHI

Radio Spectrum Laboratory, KDDI Research Inc, Fujimino-shi, Saitama 356-8502, Japan

Corresponding author: Hiromi Matsuno (hr-matsuno@kddi.com)

This work was supported by the Ministry of Internal Affairs and Communications in Japan under Grant JPJ000254.

ABSTRACT Intelligent reflecting surfaces (IRSs) have been attracting attention as a solution to coverage hole problems in millimeter-wave communication areas and are considered one of the key technologies of next-generation mobile communication systems. To utilize the IRS for mobile networks, the reflection power of the IRS should be evaluated in advance to estimate the coverage enhancement. Because the IRS becomes large, up to several tens or hundreds of wavelengths, a reflection power evaluation method for a large IRS is required. Although the reflection amplitude and phase of the reflecting element are available for the physical optics (PO)-based evaluation method, they depend on the location of the reflecting element because of the mutual coupling between adjacent reflecting elements, and should be measured at each location of the reflecting element. Since the number of reflecting elements in large IRS becomes several tens of thousands, measurement becomes difficult. In addition, although the radar cross section (RCS) is available for reflection power evaluation in the far field, a massive measurement system of several hundreds of meters is required to satisfy the far-field condition of the IRS. For these reasons, the evaluation of large IRS is challenging. To solve this problem, we propose a practical evaluation method for large IRS by synthesizing the RCS patterns of small IRSs (sub-IRSs). Since the influence of the mutual coupling between sub-IRSs depends on the size of the sub-IRSs, we formulated the mutual coupling on the IRS and evaluated the proposed method by changing the size of the sub-IRSs. The measurement results in an anechoic chamber verified that the proposed method can estimate the RCS pattern of a large IRS with a reflection power difference of less than 1dB and the correlation between the estimated RCS pattern and the actual RCS pattern exceeds more than 0.87.

INDEX TERMS Evaluation of large IRS, mutual coupling, RCS pattern, physical optics, radar equation.

I. INTRODUCTION

A. BACKGROUND

The commercial service of fifth-generation mobile communication systems (5G) is being launched on a global scale, and the technical discussions towards beyond 5G and 6G mobile communication systems have started [1]. In the beyond 5G and 6G mobile communication systems, the demands for communication qualities are expected to increase to provide highly sophisticated physical-cyber fusion [2]. To deliver such high communication qualities, the use of high-frequency bands with wide bandwidths, such as millimeter-wave bands and terahertz, is also expected to increase. However, these frequency bands suffer from severe propagation loss, especially in non-line-of-sight (NLOS) environments, because of their high path loss and high blockage loss. This creates coverage holes (dead spots) where the signal strength from a base station (BS) is insufficient to provide such high communication qualities in the communication area [3].

To overcome these problems, the use of smart repeaters, such as network-controlled repeaters (NCRs), has been attracting attention. The NCR is currently standardized in the third generation partnership project (3GPP) [4]. Since the NCR amplifies the signal from the BS, it can extend coverage.

The associate editor coordinating the review of this manuscript and approving it for publication was Olutayo O. Oyerinde.

As another approach, deploying a passive reflector is an attractive method for enhancing the coverage to reflect the signal from the BS to the coverage holes. Since it does not require an amplifier or other complicated circuits, it can enhance the coverage ecologically and economically compared to deploying additional BSs and wireless repeaters [5], [6]. In particular, by applying a meta-surface reflector, which has an artificial surface to reflect signals in the desired direction, the capability of the passive reflector is enhanced [7], [8]. Moreover, since the desired reflection direction is changed by the change of the propagation environment and user distribution [9], the intelligent reflecting surface (IRS), which can control reflection characteristics such as reflection direction and phase, has been attracting attention [4], [6], [10], [11], [12], [13], [14], [15], [16], [17], [18], [19]. Since the IRS has the capability to enhance various aspects of communication qualities, such as coverage and channel capacities, it is considered one of the key technologies of next-generation mobile communication systems [4], [10].

To utilize the IRS in mobile networks, the reflection power of the IRS must be determined in advance to estimate the coverage enhancement. Therefore, numerous studies related to the performance evaluation method of the actual IRS through measurements have been conducted [7], [8], [11], [12], [13], [14], [15], [16]. However, since the electrical size of the IRS must be large to increase the reflection power [6], [18], [19], an evaluation method for an electrically large IRS is required for practical evaluation.

B. RELATED WORKS

The IRS is designed to arrange the reflection phase in unit cells (reflecting elements) that are periodically placed at sub-wavelength intervals on the reflecting surface. The reflection power of the observation point is calculated as the sum of the reflection signal from each reflecting element. Based on this physical optics (PO) theorem, the author of [12] derived the propagation model of the IRS to evaluate the reflection power of the IRS. The electric field (E-field) from the transmitting point was multiplied by the reflection phase and amplitude (reflection coefficient) of each unit cell. The reflected E-field is synthesized at the observation point to derive the reflection power. Since the PO does not depend on the IRS size, it can be applied to an electrically large IRS.

To utilize PO for the evaluation of the actual IRS, the reflection coefficient of each unit cell should be measured correctly. The reflection coefficient of the unit cell is usually handled as the same value as the designed value, and is obtained by unit cell analysis. However, the reflecting element is affected by mutual coupling because of its short element spacing [19]. Therefore, the reflection coefficient of each reflecting element depends on the conditions of the adjacent reflecting elements. The reflection coefficient differed from the designed value. This indicates that the measurement of the reflection coefficient of each reflecting element is required to evaluate the actual IRS. However, the measured reflection signals at the observation point are the synthesized values from each unit cell, and it is difficult to derive the reflection coefficient of each unit cell. For this reason, it is difficult to apply for the evaluation of a practical IRS.

In another approach, the author of [16] derived the received power in the far-field region using the radar equation (RE). In RE, the received power is calculated using the radar cross section (RCS) of the IRS. The measured RCS includes the influence of mutual coupling; therefore, the received power of the actual IRS was evaluated. The angular characteristics of the RCS (called the RCS pattern) are obtained by changing the incident and reflection angles. Subsequently, the reflection power and direction of the actual IRS are evaluated. However, since the RCS is defined in the far-field region of the IRS, the measurement system of the RCS pattern is deployed to satisfy far-field conditions, such as the distance between the IRS and each transmitting and receiving antenna [17]. Assuming an IRS with several tens of wavelengths, a distance of more than several tens of thousands of wavelengths is required for each transmitter and receiver. Therefore, it is difficult to evaluate the actual large IRS in the RE.

C. CONTRIBUTION

To address the aforementioned problems, a practical evaluation method for an actual electrically large IRS is proposed. Since the electrically large IRS is assumed to be a combination of small IRSs (sub-IRSs) [20], the RCS pattern of the electrically large IRS is estimated by synthesizing the RCS pattern of the sub-IRS whose RCS pattern is measured in an anechoic chamber with a usual size. The reflection performance of the electrically large IRS was calculated by synthesizing the measured RCS patterns of the sub-IRSs. Since the measured RCS pattern is based on the practical performance of the sub-IRS, the calculated reflection performance of an electrically large IRS is also based on practical performance.

Here, the mutual coupling of the IRS is derived as a matrix notation using mutual impedance and array antenna theory [21], [22]. From the mutual coupling matrix, we also derived the mutual coupling matrix of the sub-IRSs and the influence of mutual coupling between sub-IRSs. With a numerical evaluation by changing the size of the sub-IRS, the influence of the mutual coupling between sub-IRSs is reduced by increasing the size of the sub-IRS. Then, the RCS pattern of the electrically large IRS is estimated by synthesizing the RCS pattern of sub-IRSs. Through the evaluation of a uniform linear array (ULA)-shaped IRS and a cross-dipole-based reflectarray [23], the validity of the proposed method was verified.

In this paper, the proposed method is verified throughout the measurement in anechoic chamber. The main contribution of the proposed paper are summerized as follows:

1) Proposal of a practical evaluation method for a large IRS using the measured RCS pattern of the sub-IRS:

The measured RCS pattern includes mutual coupling. Therefore, the proposed method can evaluate the reflection performance of a large IRS with mutual coupling.

2) Formulation of the mutual coupling matrix for the IRS and the sub-IRS:
To be utilized for PO, the mutual coupling between each reflecting element is formulated as a matrix notation.
3) Verification of proposed method using numerically calculated RCS pattern with mutual coupling matrix of ULA-shaped IRS
The synthesized RCS pattern became close to that of the electrically large RCS pattern by increasing the size of the sub-IRS.
4) Verification of proposed method with calculated RCS pattern using electromagnetic (EM) field simulator [24]
The correlation between the RCS pattern of the proposed method and the calculated data is 0.99, and the proposed method can estimate the RCS pattern of an electrically large IRS.
5) Verification of the proposed method with the measured RCS pattern in an anechoic chamber
The correlation between the RCS pattern of the proposed method and the measured data becomes 0.87 when the size of the sub-IRS is large.

D. ORGANIZATION

The remainder of this paper is organized as follows. The path-loss models used to evaluate the reflecting power are introduced in Section II. The sub-IRS synthesis method, including the formulation of mutual coupling on the IRS is proposed in Section III. In Section IV, the proposed method is numerically analyzed using a ULA-shaped IRS. In Section V, the proposed method was evaluated using the RCS pattern obtained by the EM simulator and measured in an anechoic chamber. This paper is concluded in Section VI.

II. DEFINITION OF IRS AND PATH LOSS MODEL

This section describes the IRS discussed in this paper. For simplicity, a ULA-shaped IRS was assumed. Then, the path loss model of the IRS based on the PO and RE to evaluate the reflection power is introduced.

A. DEFINITION OF IRS

Figure 1 shows the IRS discussed in this paper. The IRS is placed in the xy-plane, $(z = 0)$ as shown in the figure. The IRS consists of N reflecting elements (unit cells) arranged in the x-direction. Each reflecting element is placed within d intervals and has directivity defined as $F(\theta)$. $F(\theta)$ also includes the polarization components. When the cross polarization discrimination of the reflecting element is low, the reflecting signal strength of the co-polarization component is decreased. The angle and distance from the n-th unit cell and each transmitting and observation point are defined as $\theta_{t,n}$, $\theta_{r,n}$, r_n^t and r_n^r, respectively $(n = 1, 2, \ldots N)$. The reflection coefficient of the n-th unit cell was defined as $\Gamma_n = \alpha_n e^{j\beta_n}$. Here, each α_n and β_n denote the reflection amplitude and phase component of the n-th unit cell, respectively. Assuming the length of the unit cell in the y-direction, d, the area of the IRS is Nd^2.

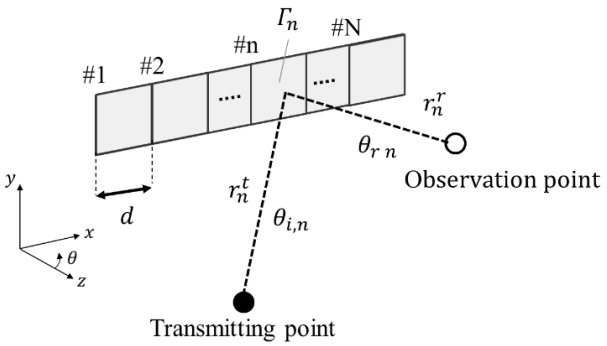

FIGURE 1. The definition of the IRS.

B. PO-BASED PATH LOSS MODEL

The path loss model of the IRS was calculated based on the PO theory [12]. The reflecting E-field at the observation point from the n-th reflecting element $E_{r,n}$ is expressed with the E-field at the transmitting point, E_t as follows:

$$E_{r,n} = \left(\frac{e^{jkr_n^t}}{r_n^t}\right) F\left(\theta_{i,n}\right) \Gamma_n F\left(\theta_{r,n}\right) \left(\frac{e^{jkr_n^r}}{r_n^r}\right) E_t, \quad (1)$$

where, $k = 2\pi/\lambda$, and λ are the wave number and wavelength, respectively. Equation (1) is converted into a matrix notation as follows:

$$\boldsymbol{E_r} = \boldsymbol{\Gamma}' E_t \quad (2)$$

$$\boldsymbol{\Gamma}' = \left[\Gamma_1', \Gamma_2', \cdots, \Gamma_M'\right] \quad (3)$$

$$\Gamma_n' = \left(\frac{e^{jkr_n^t}}{r_n^t}\right) F\left(\theta_{i,n}\right) \Gamma_n F\left(\theta_{r,n}\right) \left(\frac{e^{jkr_n^r}}{r_n^r}\right). \quad (4)$$

Assuming the transmitting power, antenna gain of each transmitting and receiving antenna, and reflecting element, P_t, G_t, G_r, and G, respectively, the received power density at the observation point, P_r, is calculated as follows [5]:

$$P_r = \frac{G_t G_r G d^2 \lambda^2}{64\pi^3} \left|\boldsymbol{E_r} \boldsymbol{E_r^T}\right|, \quad (5)$$

where $\boldsymbol{A}^T$ is the transpose matrix of $\boldsymbol{A}$. Equation (5) is the matrix notation for the PO-based received power. Since r_n^t and r_n^r are functions of the incident and reflecting angles, $\left|\boldsymbol{E_r} \boldsymbol{E_r^t}\right|$ has angle dependency.

C. RE-BASED PATH LOSS MODEL

Assuming that the distance between the IRS and each transmitting and observation point is large enough to satisfy the far-field condition of the IRS, the phase difference of each incident path length and reflecting path length, $\exp\left\{j2\pi r_n^t/\lambda\right\}$ and $\exp\left\{j2\pi r_n^r/\lambda\right\}$, becomes small and depends only on the incident and reflecting angle [16]. We define the incident and reflection angles and path

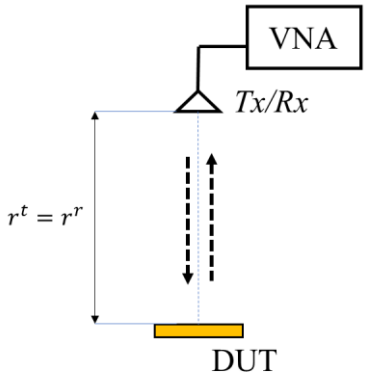

a. Reflection phase and amplitude

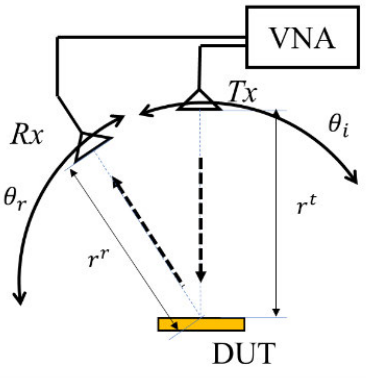

b. RCS Pattern measurement system

FIGURE 2. Conventional measurement system of the IRS.

lengths θ_t, θ_r, r^t, and r^r, respectively. Then, equations (4) and (5) are replaced as follows:

$$\Gamma'_n = F(\theta_i)\,\Gamma_n F(\theta_r)\left(\frac{e^{jkd(n-1)(sin\theta_i+\sin\theta_r)}}{r^t r^r}\right), \tag{6}$$

$$P_r = \frac{G_t G_r G d^2 \lambda^2}{64\pi^3}(E_t)^2\left|\Gamma'\Gamma'^T\right|, \tag{7}$$

$$P_r = \frac{G_t G_r d^2 \lambda^2}{64\pi^3 (r^t r^r)^2}(E_t)^2\,\sigma'(\theta_i,\theta_r). \tag{8}$$

Then the transmitting power is described with the following:

$$P_t = \frac{(E_t)^2}{(Nd^2)^2} \tag{9}$$

Therefore, equation (8) is replaced as follows:

$$P_r = P_t G_t\left(\frac{\lambda}{4\pi r^t}\right)^2 \frac{4\pi\sigma(\theta_i,\theta_r)}{\lambda^2}\left(\frac{\lambda}{4\pi r^r}\right)^2 G_r \tag{10}$$

$$\sigma(\theta_i,\theta_r) = \frac{4\pi (Nd^2)^2}{\lambda^2} D^2(\theta_i,\theta_r) \tag{11}$$

$$D(\theta_i,\theta_r) = GF(\theta_i)\,F(\theta_r)\,\Sigma_{n=1}^{N}(\Gamma_n e^{jkd(n-1)(sin\theta_i+\sin\theta_r)}) \tag{12}$$

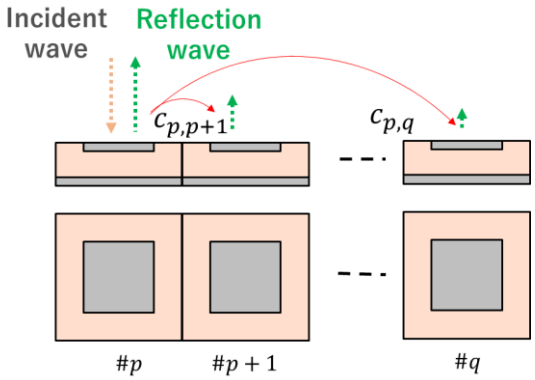

FIGURE 3. Definition of the mutual coupling on the IRS.

Equation (10) is known as the radar equation, and $\sigma(\theta_i,\theta_r)$ denote the radar cross section (RCS) of the IRS. The radar equation is expressed as a path loss model from the IRS, whose radiation power is equivalent to $P_t G_t \sigma(\theta_i,\theta_r)/r_t^2$.

III. PRACTICAL EVALUATION METHOD OF LARGE IRS

In this section, a practical evaluation method for a large IRS is proposed. Since the size of the IRS becomes large to increase the reflection power, a precise evaluation method for large IRS is required. First, the conventional evaluation method of the IRS is introduced. In the next step, the influence of mutual coupling is formulated. Subsequently, a, method for synthesizing the measured RCS pattern of the sub-IRS is proposed.

A. CONVENTIONAL EVALUATION METHOD

Through the discussion in Section II, the reflection power from the IRS was calculated using PO and RE. To precisely evaluate the reflection power, the PO requires the reflection amplitude and phase information of each unit cell, Γ_n, and the RE requires the RCS pattern of the IRS $\sigma(\theta_i,\theta_r)$. Conventional measurement systems for the IRS are shown in Fig. 2.

Figure 2a shows the monostatic measurement system. In the system, the same antenna was used for each transmitter (Tx) and received (Rx) antenna. The antenna connected to the vector network analyzer (VNA) was placed in front of the device under test (DUT). The distance between each DUT and antenna satisfies the far-field condition of the DUT. Assuming that the reference point of the VNA is at the antenna port, the measured S_{11} denotes the received power of $\theta_i = \theta_r = 0$ in equation (10). By comparing the measured S_{11} of theoretically known devices, the reflection amplitude and phase of the DUT were derived. For instance, the reflection amplitude and phase of the metal plate are known as $\alpha_{n,metal} = 1$ and $\beta_{n,metal} = \pi$. Therefore, assuming the metal plate with the same size as the DUT and consists of the same number of unit cells, the reflection amplitude and phase of

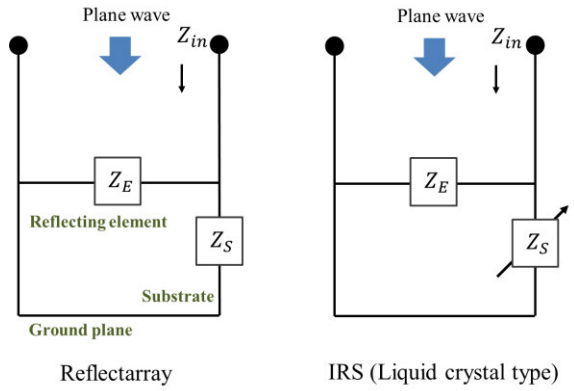

FIGURE 4. Equivalent circuit of the reflectarray and the Liquid crystal IRS [13].

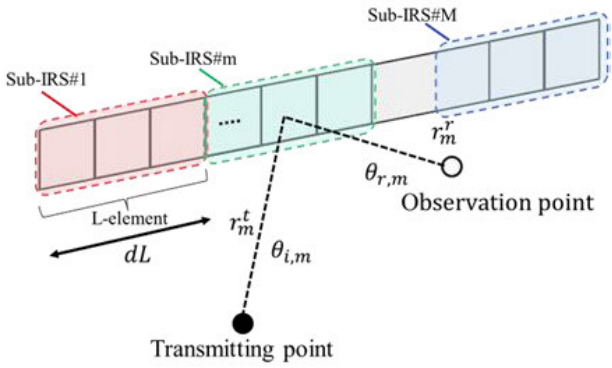

FIGURE 5. Definition of the sub-IRS.

the DUT were derived using the following equations [13]:

$$\frac{S_{11,DUT}}{S_{11,metal}} = \Sigma_{n=0}^{N} \left(\Gamma_{n,DUT} - \Gamma_{n,Metal}\right). \tag{13}$$

Equation (13) indicates that the reflecting amplitude and phase are derived as the summation of each reflecting element. Therefore, the reflection amplitude and phase are derived by measuring them as a reflecting element ($N = 1$) or averaging the same reflection amplitude and phase setting ($\Gamma_n = \Gamma$).

Figure 2b shows the bistatic measurement system. In the system, each *Tx* and *Rx* antenna is connected to the VNA. From the measured S_{21} at (θ_i, θ_r), the angular characteristics of the reflection power were obtained. Similar to the monostatic system, the RCS of the DUT was derived by comparing it withthe theoretically known DUT. For instance, assume $\theta_i = \theta_r = 0$, the RCS of a metal plate with a surface is S of $4\pi S^2/\lambda^2$. Therefore, the RCS of the DUT is derived using the following equation:

$$\sigma\left(\theta_i, \theta_r\right) = \frac{S_{21,DUT}\left(\theta_i, \theta_r\right)}{S_{21,metal}\left(0, 0\right)} \frac{4\pi S^2}{\lambda^2} \tag{14}$$

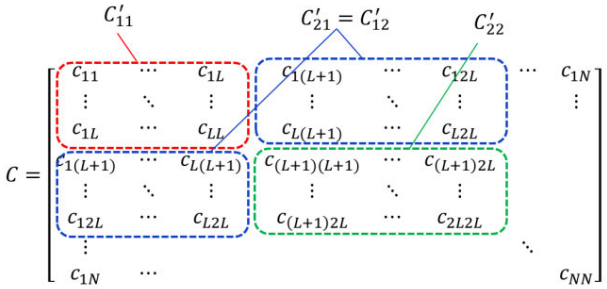

FIGURE 6. Mutual coupling matrix of sub-IRS.

B. FORMULATION OF MUTUAL COUPLING ON IRS

When current flows in the reflecting element, coupling currents are induced in the adjacent reflecting element [16]. This phenomenon is known as mutual coupling. The strength of the induced current depends on the element spacing. Since the element spacing of the IRS is generally designed within a half-wavelength, the IRS is affected by strong mutual coupling. Since the induced current also reflects the signal as shown in Fig. 3, mutual coupling distorts the reflection pattern of the IRS. Therefore, the reflection pattern, including the mutual coupling, should be evaluated. Figure 4 shows the equivalent circuits of each reflectarray and IRS. The difference between each device is whether impedance is variable or not. Therefore, the mutual coupling effect for each reflectarray and IRS is considered same.

We define the mutual coupling coefficient between the p-th and the q-th reflecting elements, $c_{p,q}$. Here, the mutual coupling coefficient is a complex value. Assuming that the IRS is composed of N reflecting elements, the influence of mutual coupling is denoted as the mutual coupling matrix $\boldsymbol{C}$,

which has $(N \times N)$ dimensions. Using the mutual coupling matrix, (2) can be converted to:

$$\boldsymbol{E}'_{\boldsymbol{r}} = \boldsymbol{C}\boldsymbol{E}_{\boldsymbol{r}}. \tag{15}$$

$$\boldsymbol{C} = \begin{bmatrix} c_{11} & \cdots & c_{1N} \\ \vdots & \ddots & \vdots \\ c_{N1} & \cdots & c_{NN} \end{bmatrix}, \tag{16}$$

Since the mutual coupling coefficient from the p-th reflecting element to the q-th reflecting element is the same as that from the q-th reflecting element to the p-th reflecting element $\left(c_{p,q} = c_{q,p}\right)$, coupling matrix $\boldsymbol{C}$ becomes a symmetrical matrix. Referring to [21], the mutual coupling is defined as a mutual impedance matrix. Therefore, when the shape of the reflecting element is designed with the same configuration, mutual coupling depends only on the element spacing of the reflecting element [22]. Based on this idea, the number of unknowns is reduced.

However, the impedance of the reflecting element is changed by changing the reflection phase, and the mutual coupling coefficient depends on both the element spacing and

reflecting coefficient Γ_n. Therefore, it is difficult to measure the reflecting phase and amplitude of an actual IRS.

C. SYNTHESIS OF RCS PATTERN OF SUB-IRS

To solve these problems, we propose an evaluation method for large IRS by synthesizing the RCS pattern of the sub-IRS. We assumed M sub-IRSs consist of L elements. Each sub-IRS was placed within dL intervals as shown in Fig. 5. The distance and angle between the m-th sub-IRS and each transmitting and observation point are defined as r_m^t, r_m^r, $\theta_{i,m}$, and $\theta_{r,m}$, respectively. When the directivity, gain, and reflecting amplitude and phase of the m-th sub-IRS are defined as $F_s\left(\theta_{i,m}\right)$, $F_s\left(\theta_{r,m}\right)$, $G_{s,m}$, and $\Gamma_{s,m}$, respectively, equation (1) is replaced as follows:

$$E_{r,m} = \left(\frac{e^{jkr_m^t}}{r_m^t}\right) F_s\left(\theta_{i,m}\right) \Gamma_{s,m} F_s\left(\theta_{r,m}\right) \left(\frac{e^{jkr_m^r}}{r_m^r}\right) E_t. \quad (17)$$

Here, since the G_s and $F_s\left(\theta_{i,m}\right)$ denote the reflection gain and directivity of the sub-IRS, respectively, they are replaced with the RCS pattern of the sub-IRS.

$$G_{s,m}\Gamma_{s,m} = \max\left(\sigma_{s,m}\left(\theta_{i,m}, \theta_{r,m}\right)\right)\left(\frac{\lambda^2}{4\pi}\right)\frac{1}{\left(Ld^2\right)^2} \quad (18)$$

$$F_s\left(\theta_{i,m}, \theta_{r,m}\right) = \frac{\sigma_{s,m}\left(\theta_{i,m}, \theta_{r,m}\right)}{G_{s,m}}. \quad (19)$$

Assuming that the distance from each *Tx* and *Rx* antenna and sub-IRS is sufficiently large to satisfy the far-field condition of the sub-IRS, the RCS pattern of the sub-IRS $\sigma\left(\theta_{i,m}, \theta_{r,m}\right)$, is measured with the system. Therefore, equations (15) and (5) are also replaced with the measured RCS pattern of the m-th sub-IRS, $\sigma_m\left(\theta_{i,m}, \theta_{r,m}\right)$ as follows:

$$E_{r,m} = \left(\frac{e^{jkr_m^t}}{r_m^t}\right)\sigma_m\left(\theta_{i,m}, \theta_{r,m}\right)\left(\frac{e^{jkr_m^r}}{r_m^r}\right)E_t. \quad (20)$$

$$P_r = \frac{G_t G_r L d^2 \lambda^2}{64\pi^3}\left|\boldsymbol{E_r}\boldsymbol{E_r^T}\right|. \quad (21)$$

Assuming a far-field region of the large IRS, the RCS pattern of the large IRS is derived from the RCS pattern of the sub-IRS.

$$D\left(\theta_i, \theta_r\right) = F\left(\theta_i\right) F\left(\theta_r\right) \Sigma_{s=1}^{S} \Sigma_{m=1}^{M} \times \left(\Gamma_m e^{jkd(m-1)\left(\sin\theta_{i,m} + \sin\theta_{r,m}\right)}\right), \quad (22)$$

$$D\left(\theta_i, \theta_r\right) = \Sigma_{m=1}^{M}\sigma_m(\theta_i, \theta_r). \quad (23)$$

D. INFLUENCE OF THE MUTUAL COUPLING

The mutual coupling matrix, was also divided into sub-IRSs as shown in Fig. 6. The mutual coupling matrix between i-th and j-th sub-IRS, C'_{ij}, is defined as

$$\boldsymbol{C'} = \begin{bmatrix} \boldsymbol{C_{11}}' & \cdots & \boldsymbol{C_{1K}}' \\ \vdots & \ddots & \vdots \\ \boldsymbol{C_{K1}}' & \cdots & \boldsymbol{C_{KK}}' \end{bmatrix}, \quad (24)$$

$$\boldsymbol{C_{ij}}' = \begin{bmatrix} c_{L(i-1)+1,(L(j-1)+1)} & \cdots & c_{L(i-1)+1,JL} \\ \vdots & \ddots & \vdots \\ c_{iL,(L(j-1)+1)} & \cdots & c_{iL,jL} \end{bmatrix}. \quad (25)$$

Here, the measured reflection pattern of sub-IRS includes the mutual coupling inside the sub-IRS, C'_{ij}, $(i = j)$. However, it does not consider the mutual coupling between each sub-IRS, C'_{ij}, $(i \neq j)$. Therefore, the proposed method handles the mutual coupling matrix as;

$$\boldsymbol{C'} = \begin{bmatrix} \boldsymbol{C_{11}}' & \boldsymbol{0} & \cdots & \boldsymbol{0} \\ \boldsymbol{0} & \boldsymbol{C_{22}}' & & \vdots \\ \vdots & & \ddots & \boldsymbol{0} \\ \boldsymbol{0} & \cdots & \boldsymbol{0} & \boldsymbol{C_{KK}}' \end{bmatrix}, \quad (26)$$

Compared to (24) and (26), the proposed method neglects the non-diagonal components of $\boldsymbol{C'}$, therefore, the reflection pattern of the proposed method is different from that of the actual IRS. By adjusting the size of the sub-IRS, the difference decreases, as discussed in the next section.

TABLE 1. Simulation specifications.

Symbol	Quantity	Values
f	Frequency	28 GHz
λ	Wavelength	10.7 mm
N	Element number	12
L	Element number of sub-IRS	2, 3, 4
D	Element spacing	0.5λ
$\theta_{i,L} = \theta_i$	Incident angle	0
$\theta_{r,L} = \theta_r$	Reflecting angle	$-90 \sim 90$
Γ_L	Reflection coefficient	-1
	Reflecting element	patch

IV. NUMERICAL EVALUATION OF MUTUAL COUPLING EFFECT

As discussed previously, the proposed method handles the non-diagonal component of the mutual coupling matrix of the sub-IRS in (24) as $\boldsymbol{0}$. This approximation causes a difference between the estimated and the actual RCS patterns. On the other hand, by increasing the size of the sub-IRS, the number of unknowns of $\boldsymbol{C_{ij}}$, which is not measured, should be decreased and the estimated RCS pattern becomes close to that of the actual RCS pattern. Therefore, the numerical evaluation results were derived by changing the sub-IRS size. To obtain consistency in the proposed method, the correlation with directivity, which is calculated using $\left|\boldsymbol{E_r}\boldsymbol{E_r^T}\right|$, the reflecting angle must be changed between the IRS and the observation point.

The simulation conditions are listed in Table 1. We assumed 12 patch-type reflecting elements with element

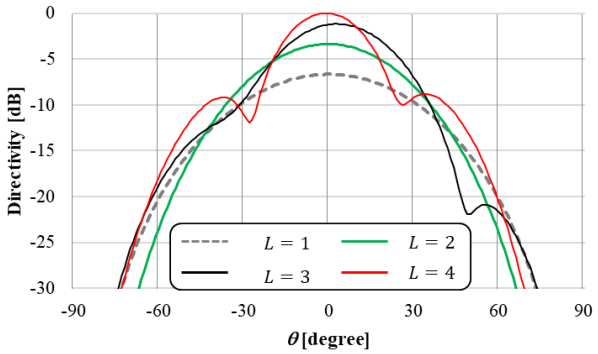

FIGURE 7. Directivity of the sub-IRS.

spacings of 0.5λ. Regarding the size of the sub-IRS, we evaluated two, three, and four-element sub-IRSs. We calculate the directivity of the sub-IRS and then estimate the directivity of the full-IRS with the directivity of the sub-IRS. For simplicity, the reflection coefficient of each reflecting element was set to -1. We assumed that the distance from the IRS and each transmitting and observation point was sufficiently large to satisfy the far-field condition. We also assumed that the transmitter was positioned in front of the IRS. Since the angle difference between each reflecting element was sufficiently small in the far-field condition, we set the incident angle of each reflecting element to the same value, $\theta_{i,k} = \theta_i = 0$. Similarly, the angle between each reflecting element and observation point was set to $\theta_{r,k} = \theta_r$. The angle dependency of the reflection power is derived by changing θ_r from -90 to 90 degrees.

Regarding mutual coupling, since the mutual coupling of the reflecting element is not derived directly, we apply the mutual coupling of the patch array calculated using [18]. As a sample, the first (4×4) components of mutual coupling matrix $C_{1:4}$, as shown at the bottom of the page.

Figure 7 shows the directivity of the sub-IRS by changing the size of the sub-IRS. $L = 1$ indicates directivity of the patch element. The directivity was normalized to $L = 4$. As shown in the figure, the directivity of $L = 1$ exhibits a peak at 0 degrees and symmetrical characteristics. On the other hand, owing to the mutual coupling effect, the directivities of each $L = 2$, 3, and 4 have asymmetrical characteristics. The asymmetry is increased with large L.

Figure 8 shows the directivity of the proposed method by changing L. Full IRS indicates the directivity calculated with the (12×12) mutual coupling matrix. Owing to mutual coupling, the directivity of the large IRS is distorted. By increasing the size of the sub-IRS, the directivity of the

TABLE 2. Measurement specifications.

Symbol	Quantity	Values
f	Frequency	28 GHz
λ	Wavelength	10.7 mm
M	Element number in the y-direction	20
N	Element number in the x-direction	6, 20, 30,
$N/2$	Element number of sub-IRS In the x-direction	3, 10, 15,
D	Element spacing	0.5λ
$\theta_{i,L} = \theta_i$	Incident angle	0
$\theta_{r,L} = \theta_r$	Reflecting angle	$-90 \sim 90$
θ_r	Reflection direction	-45
	Reflecting element	cross
r^t	Distance between DUT and Tx	2.5 m
r^r	Distance between DUT and Rx	2.0 m

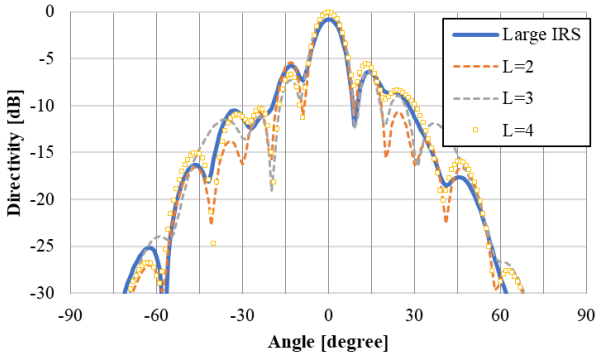

FIGURE 8. RCS pattern by changing the size of sub-IRS.

proposed method approaches that of a large IRS. The correlation between the directivity of each proposed method and a large IRS was 0.99. The difference between the directivities can be attributed to the small element numbers, N and M. In the actual IRS, the element number is assumed be increased up to more than 1,000. In this case, the size of the mutual coupling matrix also increases. However, since the influence of the mutual coupling is neglected with large element spacing, the proposed method is considered to be effective by setting sufficiently large size of sub-IRS. The effectiveness is also verified by using the IRS with several hundreds of reflecting element in the next section.

V. EVALUATION WITH META-SURFACE REFLECTOR

A. EVALUATION WITH EM SIMULATOR

To verify the validity of the proposed method, the meta-surface reflector shown in Fig. 9 was used to obtain

$$\boldsymbol{C}_{1:4} = \begin{bmatrix} 1 & -0.05+0.19j & 0.05+0.01 & -0.01+0.00j \\ -0.05+0.19j & 1 & -0.08+0.19j & -0.03+0.04j \\ 0.05+0.01j & -0.08+0.19j & 1 & -0.20-0.02j \\ -0.01+0.00j & -0.03+0.04j & -0.20-0.02j & 1 \end{bmatrix}.$$

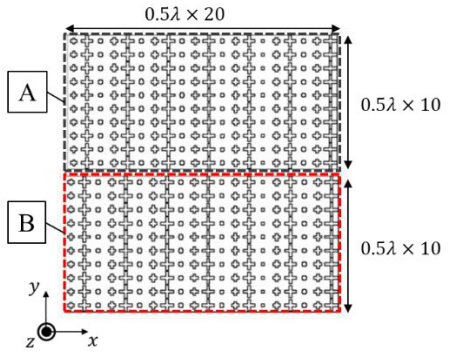

FIGURE 9. Definition of sub-IRS for simulation, each element spacing is 0.5λ at 28GHz.

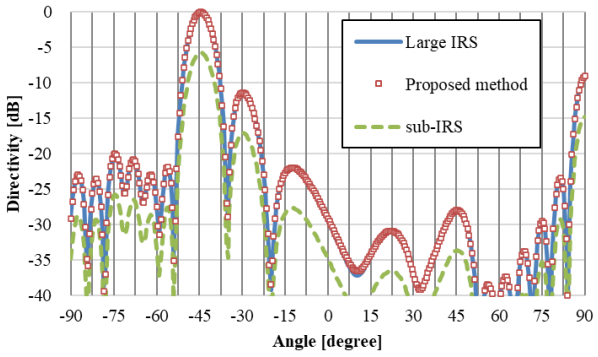

FIGURE 10. Directivity of the proposed method and large IRS using EM simulator at 28GHz.

TABLE 3. Measurement results.

Symbol	Reflection power difference	Correlation
N=6	3.2 dB	0.69
N = 20	4.9 dB	0.82
N = 30	0.83 dB	0.87

the evaluation results. The metasurface reflector consists of cross-shaped elements. Each element was placed within 0.5λ. The sub-IRS consists of 200 reflecting elements of (10 × 20) and the directivity of the large IRS with 400 reflecting elements of (20 × 20) is evaluated using the proposed method. Figure 10 shows the directivity of each proposed method and the large IRS in the zx-plane, calculated using the EM simulator. The results demonstrate that the proposed method reproduces the directivity of a large IRS.

B. EVALUATION WITH MEASURED RCS PATTERN

The validity of the proposed method is verified using the measured RCS pattern in an anechoic chamber as shown in Fig.11. The measurement conditions are listed in Table 2. The Tx antenna is set in the front of the DUT ($\theta_i = 0$) and the Rx antenna is rotated around the DUT. The distance between the DUT and each Tx and Rx antenna is set at 2.5 m and 2.0 m, respectively. Regarding the DUT, the IRS

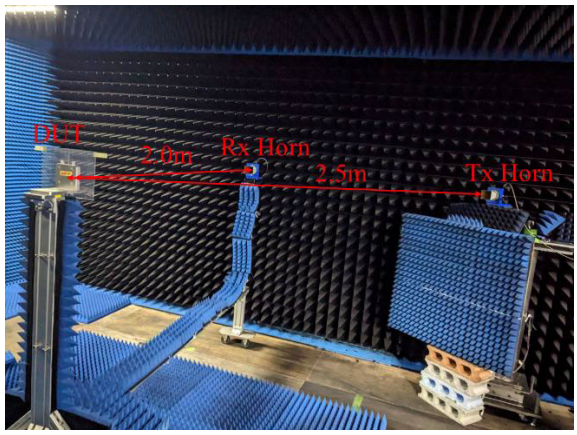

FIGURE 11. RCS pattern by changing the size of sub-IRS.

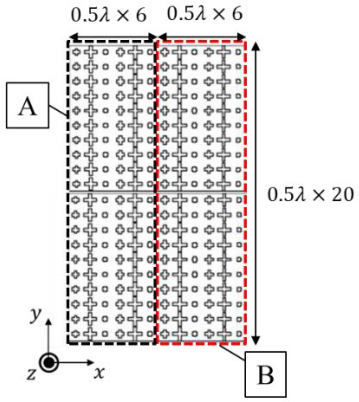

FIGURE 12. Definition of sub-IRS for measurement RCS (N=12), each element spacing is 0.5λ at 28GHz.

consists of $N \times 20$ reflecting elements ($N = 6, 20, 30$) as shown in Fig. 12. Each IRS is divided into 2 sub-IRSs whose reflecting element is $N/2 \times 20$. The RCS pattern of each sub-IRS (A, B) is measured. By synthesizing the RCS pattern of each sub-IRS, the synthesized RCS pattern is derived (A+B proposed). The synthesized RCS pattern is evaluated by comparing the measured RCS pattern (A+B measured). Figure 13 shows the measured and estimated RCS pattern. From the figure, in the case of $N = 6$, the estimated RCS pattern differs from the measured RCS pattern. The difference in the reflection power in the reflection direction ($\theta = -45$) was 3.2dB. The differences become smaller as the number of reflecting elements N increases. In the case $N > 20$, the difference becomes less than 1dB (0.74dB). In addition, the correlation between the estimated RCS pattern and the measured RCS pattern is summarized in Table 3. The reflection power difference becomes smaller with the increase of N and the correlation between the measured and estimated RCS tends to increase with a large N. These results verified that the proposed method can estimate the reflection pattern of large IRS by setting the large element number of sub-IRS.

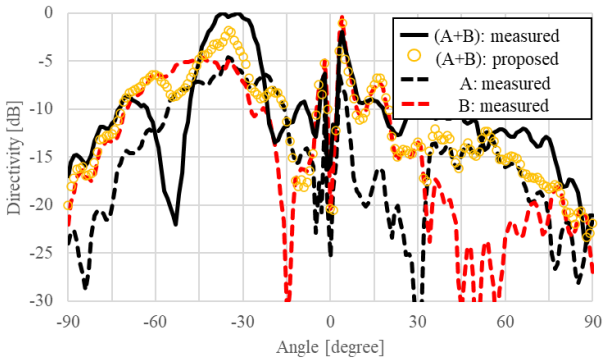

a. N=6

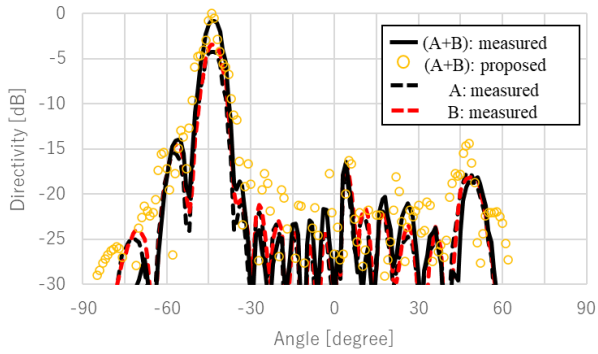

b. N = 20

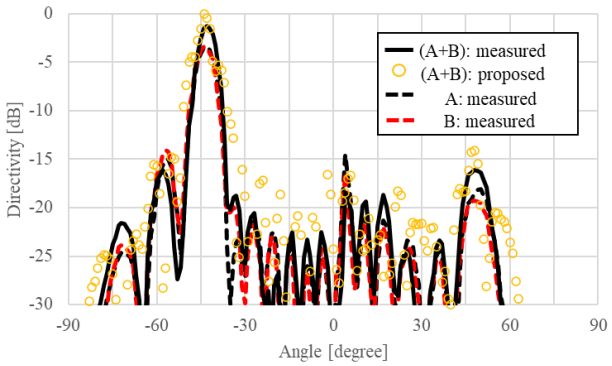

c. N= 30

FIGURE 13. Comparison of the proposed and measured RCS pattern at 28GHz.

VI. CONCLUSION

This paper proposes a practical evaluation method for electrically large IRS. Since the reflecting elements of the IRS are affected by mutual coupling from adjacent reflecting elements, measurement of the reflection coefficient of each unit cell is required to utilize PO for practical evaluation. However, it is difficult to derive the reflection coefficient of each unit cell because the measured reflecting signal is the summation of that from each reflecting element. In addition, although the RCS pattern includes the influence of mutual coupling, it is difficult to measure the RCS pattern of an electrically large IRS owing to its large far-field conditions.

To address these problems, this paper proposes an RCS pattern evaluation method by synthesizing the measured RCS pattern of the sub-IRSs. As the measured RCS pattern includes the influence of the mutual coupling, the estimated RCS pattern also includes the influence of the mutual coupling. Although there remains the influence of the mutual coupling between sub-IRSs remains, it is reduced by increasing the size of the sub-IRSs. The measurement evaluation showed that the estimated RCS pattern was in good agreement with the measured RCS pattern. The correlation between each proposed and measured RCS pattern was 0.87, which increased as the sub-IRS size increased.

REFERENCES

[1] *Studies on Frequency-Related Matters for International Mobile Telecommunications Identification Including Possible Additional Applications to the Mobile Service on Primary Basis Portion(s) of the Frequency Range Between 24.25 and 86 GHz for the Future Development of International Telecommunication for 2020 and Beyond*, document Resolution 238 WRC-15, Nov. 2015.

[2] *Key Drivers and Research Challenges for 6G Ubiquitous Wireless Intelligence*, 6G Flagship, Univ. Oule, Oulu, Finland, Sep. 2019.

[3] S. Rangan, T. S. Rappaport, and E. Erkip, "Millimeter-wave cellular wireless networks: Potentials and challenges," *Proc. IEEE*, vol. 102, no. 3, pp. 366–385, Mar. 2014.

[4] Y. Yuan, D. Wu, Y. Huang, and I. Chih-Lin, "Reconfigurable intelligent surface relay: Lessons of the past and strategies for its success," *IEEE Commun. Mag.*, vol. 60, no. 12, pp. 117–123, Dec. 2022.

[5] C. K. Anjinappa, F. Erden, and I. Güvenç, "Base station and passive reflectors placement for urban mmWave networks," *IEEE Trans. Veh. Technol.*, vol. 70, no. 4, pp. 3525–3539, Apr. 2021.

[6] M. Di Renzo, K. Ntontin, J. Song, F. H. Danufane, X. Qian, F. Kazarakis, J. D. Rosny, D. Phan-Huy, O. Simeone, R. Zhang, M. Debbah, G. Lerpsey, and S. Shamai, "Reconfigurable intelligent surfaces vs. relaying: Differences, similarities, and performance comparison," *IEEE Open J. Commun. Soc.*, vol. 1, pp. 798–807, 2020.

[7] H. Matsuno, T. Ohto, and T. Hayashi, "Development of intelligent reflecting surfaces for mobile communication systems," in *Proc. IEEE Int. Workshop Electromagn., Appl. Student Innov. Competition (iWEM)*, Aug. 2022, pp. 5–6.

[8] T. Hongnara, Y. Shirasawa, T. Sasaki, K. Sasaki, K. Sato, I. Oshima, N. Michishita, H. Nakabayashi, and K. Cho, "Dual-polarized broad-beam reflective metasurface based on multi-sheet configuration for local 5G application at 28.25 GHz," in *Proc. 15th Eur. Conf. Antennas Propag. (EuCAP)*, Mar. 2021, pp. 1–4.

[9] A. Gómez-Andrades, R. Barco, and I. Serrano, "A method of assessment of LTE coverage holes," *EURASIP J. Wireless Commun. Netw.*, vol. 2016, no. 1, pp. 1–12, Dec. 2016.

[10] M. Jian, R. Liu, and Y. Chen, "Standardization for reconfigurable intelligent surfaces: Progresses, challenges and the road ahead," in *Proc. IEEE/CIC Int. Conf. Commun. China (ICCC Workshops)*, Jul. 2021, pp. 337–342.

[11] E. Basar, M. Di Renzo, J. de Rosny, M. Debbah, M.-S. Alouini, and R. Zhang, "Wireless communications through reconfigurable intelligent surfaces," *IEEE Access*, vol. 7, pp. 116753–116773, 2019.

[12] W. Tang, M. Z. Chen, X. Chen, J. Y. Dai, Y. Han, M. D. Renzo, Y. Zheng, S. Jim, Q. Cheng, and T. J. Cui, "Wireless communications with reconfigurable intelligent surface: Path loss modeling and experimental measurement," *IEEE Trans. Wireless Commun.*, vol. 20, no. 1, pp. 421–439, Jan. 2021.

[13] H. Matsuno, T. Ohto, T. Hayashi, Y. Amano, M. Okita, D. Suzuki, K. Matsunaga, and S. Oka, "Development of a dual-polarized direction-variable liquid-crystal meta-surface reflector for intelligent reflecting surface," *IEEE Access*, early access, May 15, 2023, doi: 10.1109/ACCESS.2023.3276231.

[14] Ö. Özdogan, E. Björnson, and E. G. Larsson, "Intelligent reflecting surfaces: Physics, propagation, and pathloss modeling," *IEEE Wireless Commun. Lett.*, vol. 9, no. 5, pp. 581–585, May 2020.
[15] M.-A. Richards, *Fundamentals of Radar Signal Processing*, 2nd ed. New York, NY, USA: McGraw-Hilll, 2014.
[16] W. Tang, X. Chen, M. Z. Chen, J. Y. Dai, Y. Han, M. Di. Renzo, S. Jin, Q. Cheng, and T. J. Cui, "Path loss modeling and measurements for reconfigurable intelligent surfaces in the millimeter-wave frequency band," *IEEE Trans. Commun.*, vol. 70, no. 9, pp. 6259–6276, Sep. 2022.
[17] M. Di Renzo, F. H. Danufane, X. Xi, J. de Rosny, and S. Tretyakov, "Analytical modeling of the path-loss for reconfigurable intelligent surfaces—Anomalous mirror or scatterer?" in *Proc. IEEE 21st Int. Workshop Signal Process. Adv. Wireless Commun. (SPAWC)*, May 2020, pp. 1–5.
[18] M. Najafi, V. Jamali, R. Schober, and H. V. Poor, "Physics-based modeling of large intelligent reflecting surfaces for scalable optimization," *IEEE Trans. Commun.*, vol. 69, no. 4, pp. 2673–2691, Apr. 2021.
[19] R. J. Williams, E. de Carvalho, and T. L. Marzetta, "A communication model for large intelligent surfaces," in *Proc. IEEE ICC Workshops*, Jun. 2020, pp. 1–6.
[20] H. Matsuno, T. Nagao, T. Ohto, T. Hayashi, and M. Harada, "Practical evaluation method for large IRS: RCS pattern synthesis of sub-IRS with mutual coupling," in *Proc. IEEE 96th Veh. Technol. Conf. (VTC-Fall)*, Sep. 2022, pp. 1–4.
[21] I. Gupta and A. Ksienski, "Effect of mutual coupling on the performance of adaptive arrays," *IEEE Trans. Antennas Propag.*, vol. AP-31, no. 5, pp. 785–791, Sep. 1983.
[22] Z. Zheng, K. Liu, W.-Q. Wang, Y. Yang, and J. Yang, "Robust adaptive beamforming against mutual coupling based on mutual coupling coefficients estimation," *IEEE Trans. Veh. Technol.*, vol. 66, no. 10, pp. 9124–9133, Oct. 2017.
[23] L. Wang, H. Hagiwara, Y. Rikuta, T. Kobayashi, H. Matsuno, T. Hayashi, S. Ito, and M. Nakano, "Experimental investigation of optically transparent dual-polarized reflectarray with suppressed sidelobe level," in *Proc. Int. Symp. Antennas Propag. (ISAP)*, Jan. 2021, pp. 407–408.
[24] Dassault Systems. *CST Studio Suite*.

HIROMI MATSUNO received the B.E., M.E., and Ph.D. degrees from Yokohama National University, Japan, in 2005, 2007, and 2010, respectively. After joining KDDI Research and Development Laboratories (currently KDDI Research Inc.), in 2010, he was engaged in research and development in the field of base station antennas for fourth and fifth-generation mobile communication systems. In 2015, he joined the Advanced Telecommunication Research Institute International (ATR), where he was engaged in the field of dynamic spectrum sharing and localization. In 2018, he joined KDDI Research Inc. He is currently involved in research and development in the field of intelligent reflecting surfaces and antennas for beyond 5G/6G mobile communication systems. He received the Meritorious Award on Radio from the Association of Radio Industries and Businesses (ARIB), in 2021.

TAKUYA OHTO (Member, IEEE) received the B.E. degree in electrical and electronic engineering from Kyoto University, in 2015, and the M.E. degree from the Graduate School of Informatics, Kyoto University, in 2017. He was an employee of KDDI Corporation. In 2020, he joined KDDI Research Laboratories Inc. His current research interests include millimeter-wave wireless communications and reconfigurable intelligent surfaces. He is a member of the IEICE.

TOMOFUMI KANNO received the B.E. and M.E. degrees in science and engineering from Saitama University, in 2018 and 2020, respectively. In 2022, he joined KDDI Research Inc. He is currently engaged in the field of meta-surfaces and antennas for beyond 5G/6G mobile communication systems.

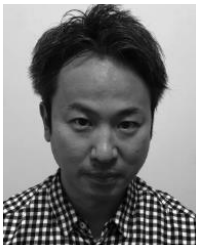

TAKAHIRO HAYASHI received the B.E. and M.E. degrees in information and communication engineering from Yokohama National University, Japan, in 2002 and 2004, respectively. In 2004, he joined KDDI Corporation, where he was engaged in telecommunication network planning and optimization. Since 2010, he has been engaged in the research and development of mobile communication systems with KDDI Research Inc. He is currently involved in the development of new frequency bands and radio propagation prediction by using machine learning. He received the Young Researcher's Award from IEICE, in 2011.